Frequency Diverse Array Spatial Data Focusing: Free Space and Multipath Experimental Validation

Guylian Molineaux*†, François Horlin*, Muriel Darces†, Philippe De Doncker*, Julien Sarrazin†
*OPERA – Wireless Communications Group
Université Libre de Bruxelles, 1050 Brussels, Belgium
†CNRS, Laboratoire de Genie Electrique et Electronique de Paris
Sorbonne Université, 75005 Paris, France
Univ. Paris-Saclay, CentraleSupélec, 91192 Gif-sur-Yvette, France

***Abstract*—This paper presents the first-ever experimental validation of both spatial data focusing (SDF) and time-invariant frequency diverse array (FDA) range-angle-based focusing, in both free space and multipath environments. In particular, a hybrid FDA-based SDF (FDA-SDF) approach is considered for spatially confined broadcasting, i.e. geocasting. First, the base FDA-SDF free space system model is reviewed. Next, a novel OFDM-based FDA-SDF system model is introduced to ensure robust operation in multipath channels. The schemes are validated, respectively, in an anechoic chamber and outdoor measurement setup using software defined radios. Results confirm FDA-SDF's anticipated supreme spatial precision: a $0.9\,\mathrm{m} \times 4.0^\circ$ range-azimuth geocast delivery zone is generated by a 4-antenna array in free space. Additionally, they illustrate that OFDM-based FDA-SDF provides all necessary performance improvements for practical operation in outdoor multipath environments. Most notably, FDA-SDF is shown to overcome the time-variance flaw of conventional FDA.**

***Index Terms*—Frequency diverse array (FDA), spatial data focusing (SDF), geocasting, experimental validation.**

I. Introduction

Geocasting, or location-based multicasting, is the spatially confined broadcasting of information towards users within a designated and restricted geographical area. It enables location-based services or messaging to large groups of mobile devices for applications such as advertising, tourism, emergency communications, or traffic management in the context of internet-of-things or smart cities. It is commonly implemented at the network layer through geographic routing algorithms that integrate physical location information into logical network addressing [1]. However, these approaches often require self-localizing nodes and are subject to multi-hop forwarding delays and trade-offs between scalability, overhead, and delivery rate. Alternatively, to avoid these shortcomings, geocasting can be enforced directly at the physical layer by exploiting base station spatial focusing techniques that manipulate the spatial bit error rate (BER) distribution to generate a geocast delivery zone.

Beamforming is an evident candidate to realize the above scenario of physical-layer multicasting [2] or geocasting [3]. It exploits interference between signals transmitted from an array to perform spatial power focusing that manipulates the signal-to-noise ratio (SNR), and thereby the BER, according to the array radiation pattern to generate a geocast delivery zone. Although classical phased array (PA) is limited to angular beamforming, frequency diverse array (FDA) can achieve range-angle-dependent beamforming by varying the carrier frequency of antennas along the array. While original linear FDA [4] is unfit for geocasting as it yields unbounded and range-angle-coupled beampatterns, nonlinear FDA schemes, such as logarithmic FDA [5] or random FDA [6], allow for range-angle-decoupling of FDA beampatterns to generate an isolated geocast delivery zone. Furthermore, FDA is often equipped with directional modulation (DM) techniques to mitigate sidelobes of elevated SNR that otherwise allow data recovery outside the geocast delivery zone [7], [8]. Nevertheless, just as PA, FDA remains limited by beamforming's inherent requirement for large physical arrays to obtain high spatial precision.

Additionally, supported by a lack of experimental validation for FDA range-angle-based focusing, recent work [9] has exposed that FDA beampatterns are time-variant in range such that they cannot deliver the anticipated range-confined wireless communications. Nevertheless, [9] considers only the above described classical beamforming FDA approaches that rely on radio frequency (RF) radiation pattern manipulation for power focusing. On the other hand, an additional degree of freedom to circumvent FDA time-variance at RF is obtained when considering orthogonal signal transmission complemented by cooperative multi-frequency down-conversion from RF to baseband, as in single-antenna multi-channel receivers [10], [11]. However, to the best of the authors' knowledge, these approaches lack experimental validation, just as conventional FDA. In addition, by mimicking the FDA beamforming array factor in baseband, they redundantly employ orthogonal resources for retransmission of identical information and, moreover, fail to overcome its spatial precision limitations.

Spatial data focusing (SDF), on the other hand, releases beamforming's power focusing constraints entirely and directly addresses the geocasting scenario. In particular,

This work was supported by the ANR GEOHYPE project, grant ANR-16-CE25-0003 of the French Agence Nationale de la Recherche, and carried out in the framework of COST Action CA20120 INTERACT. G. Molineaux is a FRIA grantee of the Fonds de la Recherche Scientifique – FNRS.

it performs distributed and orthogonal transmission of information from an array, employing dedicated equalization at cooperative receivers to induce a location-dependent symbol distortion that restricts the geographic area of correct data recovery. This fundamentally different approach allows it to significantly increase focusing precision and reduce array size. This was first demonstrated in the angular domain by time-based SDF (T-SDF) [12] that uses time-orthogonal distributed transmission. It was extended to the range domain by exploiting OFDM subcarrier orthogonality and frequency diversity in OFDM-based SDF (OFDM-SDF) [13], [14]. Moreover, a hybrid FDA-based SDF (FDA-SDF) approach has been proposed in [15], [16]. It has shown to simultaneously improve (i) design flexibility over OFDM-SDF and (ii) focusing precision over conventional beamforming-based FDA. Most importantly, SDF's inherent orthogonal baseband signal processing enables it to naturally and more efficiently mitigate FDA time-variance.

Nevertheless, FDA-SDF models in [15], [16] are limited to free space scenarios such that they cannot guarantee correct operation in multipath environments; moreover, just like the aforementioned standalone FDA or SDF approaches, they lack experimental validation that affirms their prospects for practical applications. Therefore, this paper presents an extended FDA-SDF approach that exploits OFDM features to guarantee proper SDF behavior in multipath scenarios. Additionally, both the free space and multipath FDA-SDF schemes are validated experimentally using a setup of software defined radios (SDRs), respectively in an anechoic chamber and outdoor scenario. Hence, this paper's contribution is threefold:

- novel *OFDM-based FDA-SDF system model*, providing FDA-SDF robustness in multipath channels;
- first-ever reported *experimental validation of FDA* time-invariant range-angle-based focusing;
- first-ever reported *experimental validation of SDF*, both in free space and multipath environments.

Section II summarizes the free space FDA-SDF system model (Section II-A) and enhances it for multipath channels (Section II-B). Section III describes the experimental setup for both scenarios. The results and performance are discussed in Section IV. Section V concludes the paper.

II. System Model

Fig. 1 shows the FDA-SDF system model considered in this paper. At the transmitter, it employs an N-antenna linear array with uniform spacing b, antenna indexing $n = 0, 1, \ldots, N-1$, and the origin defined at antenna $n = 0$. For FDA operation, the carrier frequency f_n at each antenna n varies from a base carrier frequency f_c by a small frequency offset Δf_n, i.e. $f_n = f_c + \Delta f_n$, with $\Delta f_n \ll f_c$. A single-antenna receiver is located at polar coordinates (d, θ), with d the radial distance to the array origin and θ the azimuth angle with respect to the array broadside direction. A free space FDA-SDF system model has already been presented by the authors in [15], [16]. However, to clarify its expansion to multipath channels in Section II-B and its experimental validation in Sections III-A and IV-A, it is briefly reviewed below.

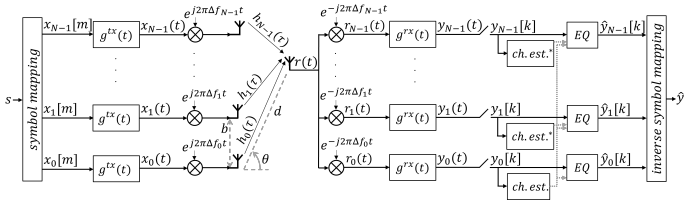

Fig. 1. FDA-based spatial data focusing system model. Channel estimation blocks marked by a * are required only in multipath scenarios (Section II-B).

A. Free Space

For SDF operation, FDA-SDF performs distributed and orthogonal transmission of information from the different FDA antennas. Specifically, an arbitrary symbol stream s is remapped to N disjoint and exhaustive symbol substreams s_n. For simplicity, the same alternating and cyclic symbol mapping as in [15], [16] is assumed, i.e. $s_n[m] = s[mN+n]$, with $m \in \mathbb{N}$ the substream symbol index. The symbols $x_n[m]$ to be transmitted from the n-th FDA antenna are then defined from the corresponding SDF symbol substream $s_n[m]$ as

$$x_n[m] = s_n[m]e^{j\varphi_n^{steer}} = s[mN+n]e^{j\varphi_n^{steer}}, \qquad (1)$$

where a steering phase φ_n^{steer} is added to enable manipulation of the geocast delivery zone location, as detailed in [15], [16]. The symbols $x_n[m]$ are transmitted sequentially from the array by modulation onto a transmitter waveform $g^{tx}(t)$, with t the time variable, orthogonally time-shifted according to the symbol mapping. Given a symbol period $T = \frac{1}{F_d}$, for a symbol rate F_d, the baseband transmitted signal $x_n(t)$ for each antenna n is then given by

$$x_n(t) = \sum_m x_n[m]g^{tx}(t - mNT - nT). \qquad (2)$$

For time-invariant FDA operation, a symmetric 2-stage multi-frequency up and down-conversion is then required [15], [16]. At the transmitter, the signals $x_n(t)$ are first individually up-converted by their respective frequency offsets Δf_n, followed by collective up-conversion by the common base carrier frequency f_c, to yield the desired RF carrier $f_n = f_c + \Delta f_n$ at each antenna n. Reversely, at the receiver, the incoming aggregated RF signal is first down-converted by the common base carrier frequency f_c, before separate further down-conversion by each of the frequency offsets Δf_n. The RF propagation channel for each antenna n can then be modeled at the common carrier frequency f_c by the baseband channel impulse response (CIR). In free space, it is given by

$$h_n^{los}(\tau) = \alpha\delta(\tau - \tau_n)e^{-j2\pi f_c\tau_n}, \qquad (3)$$

where $\delta(\cdot)$ is the Dirac delta function, τ the delay variable, τ_n the n-th channel's propagation delay, and α the complex amplitude (assumed identical in all channels for close antenna spacing). As such, assuming that transmitter-receiver carrier

offsets are absent for cooperative geocasting receivers synchronized and calibrated to the transmitter, the received baseband signals $r_v(t)$, obtained after separate down-conversion by the respective frequency offsets Δf_v, $v = 0, 1, \ldots, N-1$, are given by

$$r_v(t) = \Big[\sum_n \big(x_n(t) e^{j2\pi \Delta f_n t} \big) * h_n^{los}(\tau) + z(t) \Big] e^{-j2\pi \Delta f_v t} \quad (4a)$$

$$= \sum_n \alpha x_n(t - \tau_n) e^{-j2\pi f_n \tau_n} e^{j2\pi \Delta f_{nv} t} + z_v(t) \quad (4b)$$

$$= \sum_n \big(x_n(t) * \tilde{h}_n^{los}(\tau) \big) e^{j2\pi \Delta f_{nv} t} + z_v(t), \quad (4c)$$

where $*$ is the convolution operator, $z(t) \sim \mathcal{CN}(0, \sigma_z^2)$ models complex additive white Gaussian noise, and $z_v(t)$ is the noise after frequency down-conversion by Δf_v. From (4c), one finds that the perceived CIR $\tilde{h}_n^{los}(\tau) = \alpha \delta(\tau - \tau_n) e^{-j2\pi f_n \tau_n}$ for the n-th FDA antenna is characterized by the desired FDA phase and that FDA time-variance due to up and down-conversion frequency offset mismatches $\Delta f_{nv} = \Delta f_n - \Delta f_v = f_n - f_v$ affects only signal components $x_n(t)$ for which $n \neq v$.

At the receiver, demodulation then allows to exploit the transmitter waveform orthogonality to extract the desired time-invariant signal components $x_v(t)$ from each corresponding received signal $r_v(t)$ [15], [16]. First, the demodulated signals $y_v(t)$ are obtained by convolution of the signals $r_v(t)$ with a receiver waveform $g^{rx}(t)$, yielding

$$y_v(t) = r_v(t) * g^{rx}(t) \quad (5a)$$

$$= \sum_n \alpha e^{-j2\pi f_n \tau_n} \Bigg\{ \sum_m x_n[m] \times \Big[\big(g^{tx}(t - \tau_n - mNT - nT) e^{j2\pi \Delta f_{nv} t} \big) * g^{rx}(t) \Big] \Bigg\} \quad (5b)$$

$$+ z'_v(t),$$

where $z'_v(t)$ is the demodulated noise. The k-th received symbol $y_v[k]$ from the v-th substream is then extracted by sampling the demodulated signal $y_v(t)$ according to the transmitter symbol mapping and time-shift, i.e. at $t = \tau_0 + kNT + vT$. To this end, the waveforms $g^{tx}(t)$ and $g^{rx}(t)$ should preserve inter and intra-antenna signal orthogonality in (5b), despite the time-variant FDA phases $e^{j2\pi \Delta f_{nv} t}$. As shown in [16], this is ensured in a matched filtering approach, i.e. $g^{tx}(t) = g(t)$ and $g^{rx}(t) = g^*(-t)$, for any filter $g(t)$ of span below the symbol period T. One finds

$$y_v[k] = \alpha x_v[k] e^{-j2\pi f_v \tau_v} + z'_v[k], \quad (6)$$

where $z'_v[k]$ is the sampled noise and sampling offsets due to inter-antenna delay differences are neglected under the narrowband assumption $|\tau_n - \tau_0| \ll T$.

SDF then equalizes the received FDA symbols (6) from all channels using the same unique estimation of the channel $n = 0$ at the array origin, referred to as the reference channel. By denoting the delay and frequency difference between the n-th and reference channel as, respectively, $\Delta\tau_n = \tau_n - \tau_0$ and $\Delta f_n = f_n - f_0 = f_n - f_c$, assuming – without loss of generality – that the reference antenna carrier frequency f_0 is equal to the base carrier frequency f_c, one finds that simple zero forcing (ZF) equalization yields the following expression for the m-th equalized received symbol from the n-th antenna[1]

$$\hat{y}_n[m] = s_n[m] e^{j\varphi_n^{steer}} e^{-j2\pi f_0 \Delta\tau_n} e^{-j2\pi \Delta f_n \tau_n} + \hat{z}_n[m], \quad (7)$$

where $\hat{z}_n[m]$ is the equalized noise sample and $x_n[m]$ was substituted according to (1). The delay and frequency offset, $\Delta\tau_n$ and Δf_n, between the equalized and reference channel thus cause a residual phase shift on the equalized symbols (7) that depends on the receiver position (d, θ) through τ_n and $\Delta\tau_n$. For FDA-SDF geocasting receivers, correct recovery of the entire received symbol stream $\hat{y}[mN + n] = \hat{y}_n[m]$ (obtained by inverting the transmitter symbol mapping) is thus limited to the geographical location(s) where the residual phase shift in (7) is collectively zero for the received symbols $\hat{y}_n[m]$ from all antennas n. Around this location, a geocast delivery zone of sub-threshold BER is generated. An extensive analytical description of its geographical properties is given in [16].

B. Multipath Channels

Despite significant improvement over conventional FDA's spatial focusing precision shown in [15], [16], the system model in Section II-A is unfit for operation in multipath environments. Besides the typical frequency-selective fading and inter-symbol interference, time-dispersive multipath propagation degrades FDA-SDF performance in particular by (i) violating the inter and intra-antenna orthogonality conditions required for time-invariant baseband FDA symbol extraction from (5b), and (ii) distorting the ideal and spatially tractable line-of-sight (LOS) phase shift required for location-based SDF operation in (7). The proposed novel OFDM-based FDA-SDF system model, with modified SDF channel estimation and equalization, mitigates both aforementioned shortcomings of the free space FDA-SDF model, as detailed below. In this OFDM context, a total bandwidth $B = QB_c$ is assumed, with Q the number of subcarriers and B_c the subcarrier bandwidth.

1) Transmitter-side Signal Processing: In OFDM-based FDA-SDF, distributed transmission of information is enforced at the OFDM block-level by remapping an arbitrary stream of OFDM blocks S to N disjoint and exhaustive OFDM block substreams S_n. As in Section II-A, an alternating and cyclic mapping is adopted, i.e. $S_n[q, u] = S[q, uN + n]$, with $u \in \mathbb{N}$ the substream OFDM block index and $q = -\frac{Q}{2}, \ldots, \frac{Q}{2} - 1$ the subcarrier index. Analogous to (1), the OFDM blocks $X_n[q, u]$ to be transmitted from the n-th FDA antenna are defined as

$$X_n[q, u] = S_n[q, u] e^{j\varphi_n^{steer}} = S[q, uN + n]^{j\varphi_n^{steer}}. \quad (8)$$

[1]Given that sampling extracts a unique symbol with index $m = k$ from antenna $n = v$, the indices m and n suffice to unambiguously identify both the transmitted and received symbols.

2) Propagation Channel Model: Note that the proposed OFDM-based FDA-SDF approach remains compatible with the base FDA-SDF system model in Fig. 1. Indeed, in this scenario, the FDA input symbols $x_n[m]$ correspond to the serialized time-domain samples after inverse discrete Fourier transform of the OFDM blocks $X_n[q,u]$ and subsequent cyclic prefix (CP) insertion. The baseband transmitted signals $x_n(t)$ are then simply constructed from the corresponding symbols $x_n[m]$ by adjusting the transmitter time-shift in (2) to the OFDM block-wise symbol mapping.[2] As such, (4c) remains suited for describing the baseband FDA received signals $r_v(t)$, where, under the assumption of a linear time-invariant multipath channel, the free space perceived CIR $\tilde{h}_n^{los}(\tau)$ can be replaced by its multipath equivalent $\tilde{h}_n(\tau)$. Considering a LOS component $l=0$ and an arbitrary number $L_n \in \mathbb{N}$ of multipath components $l=1,2,\dots,L_n$ in each channel n, characterized by their propagation delay $\tau_n^{(l)}$ and complex amplitude $\alpha_n^{(l)}$, the latter is given by

$$\tilde{h}_n(\tau) = \alpha_n^{(0)}\delta(\tau-\tau_n^{(0)})e^{-j2\pi f_n \tau_n^{(0)}} + \sum_{l=1}^{L_n} \alpha_n^{(l)}\delta(\tau-\tau_n^{(l)})e^{-j2\pi f_n \tau_n^{(l)}}. \tag{9}$$

Upon demodulation as in (5a), considering the OFDM block-wise transmitter symbol mapping and time-shift, the conventional prerequisite that the OFDM CP length exceeds the channel delay spread to prevent inter-block interference then simultaneously ensures that inter and intra-antenna orthogonality for time-invariant FDA is preserved. Therefore, the conventional OFDM multiplicative frequency-domain channel model can be adopted for OFDM-based FDA-SDF.

To this end, the multipath channel transfer function $\tilde{H}_n(f)$ is calculated from the above CIR (9). Considering time-acquisition with respect to the reference channel LOS delay $\tau_0^{(0)}$ and writing $\tau_n^{(l)} = \tau_0^{(0)} + \Delta\tau_n^{(l)}$, with $\Delta\tau_n^{(0)} \ll T$, one finds

$$\tilde{H}_n(f) = \alpha_n^{(0)} e^{-j2\pi f_n \tau_n^{(0)}} + \sum_{l=1}^{L_n} \alpha_n^{(l)} e^{-j2\pi f_n \tau_n^{(l)}} e^{-j2\pi f \Delta\tau_n^{(l)}}, \tag{10}$$

where f is the baseband frequency. Assuming a frequency-flat channel $\tilde{H}_n[q] = \tilde{H}_n(qB_c)$ for each subcarrier q, the OFDM blocks received from the n-th antenna are then given by

$$Y_n[q,u] = \tilde{H}_n[q]X_n[q,u] + Z_n[q,u], \tag{11}$$

where $Z_n[q,u] \sim \mathcal{CN}(0,\sigma_z^2)$ models complex additive white Gaussian noise with variance σ_z^2.

3) Receiver-side Signal Processing: From (10) it is clear that, as anticipated, multipath distortion of the LOS phase prevents conventional SDF ZF equalization of the received OFDM blocks (11) by a reference channel estimation $\hat{H}_0[q]$ from yielding the desired residual phase shift of the free space FDA-SDF equalized symbols (7). Therefore, just like OFDM-SDF in [14], a 2-stage equalization is required to emulate this desired behavior and ensure that the free space geographical FDA-SDF properties from [16] remain valid. Specifically, the n-th antenna's equalized OFDM blocks are computed as

$$\hat{Y}_n[q,u] = Y_n[q,u] \underbrace{\frac{1}{\hat{H}_n[q]}}_{\text{(i)}} \underbrace{\frac{\hat{H}_n^{los}}{\hat{H}_0^{los}}}_{\text{(ii)}}, \tag{12}$$

where (i) classic OFDM ZF equalization by the proper n-th channel estimation $\hat{H}_n[q]$ mitigates multipath distortion, and (ii) the ideal spatially tractable free space FDA-SDF residual phase shift is emulated using estimations $\hat{H}_n^{los}$ and $\hat{H}_0^{los}$ of, respectively, the n-th and reference channel's LOS component.

The aggregated channel estimations $\hat{H}_n[q]$ are obtained via conventional OFDM unsteered preamble transmission from each antenna n. Inverse discrete Fourier transform then yields each channel's CIR estimation, used to deduce the LOS component estimations $\hat{H}_n^{los}$. Specifically, considering the limited OFDM bandwidth B, the channel transfer function (10) yields that the first tap of the n-th channel's estimated CIR is given by

$$\hat{h}_n[0] = \alpha_n^{(0)} e^{-j2\pi f_n \tau_n^{(0)}} + \sum_{l=1}^{L_n} \alpha_n^{(l)} \operatorname{sinc}\left(B\Delta\tau_n^{(l)}\right) e^{-j2\pi f_n \tau_n^{(l)}} + \epsilon_n[0], \tag{13}$$

where $\epsilon_n[0]$ represents the n-th CIR's first tap noise-induced estimation error. Thus, (13) holds the desired LOS phase information $\angle\tilde{h}_n^{los} = -2\pi f_n \tau_n^{(0)}$ of the free space perceived FDA CIR $\tilde{h}_n^{los}(\tau)$, albeit subject to multipath and estimation error disturbances. Nevertheless, one notes that the expected LOS phase difference between two antennas n_1 and n_2, given by

$$\angle\tilde{h}_{n_2}^{los} - \angle\tilde{h}_{n_1}^{los} = -2\pi\big(\Delta f_{n_2} - \Delta f_{n_1}\big)\tau_0^{(0)} - 2\pi\big(n_2 f_{n_2} - n_1 f_{n_1}\big)\Delta\tau^{(0)}, \tag{14}$$

is linear with respect to the reference channel LOS delay $\tau_0^{(0)}$ and LOS delay difference $\Delta\tau^{(0)}$ of neighboring channels, where $\Delta\tau_n^{(0)} = n\Delta\tau^{(0)}$ was used given the uniform antenna spacing. By design, (13)'s phase must thus adhere to the same, but disturbed, linear relationship. As such, observations of the estimated CIR first tap phase difference for pairs of antennas $(n_1^1, n_2^1), \dots, (n_1^I, n_2^I), I \in \mathbb{N}, I \geq 2$ allow to determine least squares estimations $\hat{\tau}_0^{(0)}$ and $\Delta\hat{\tau}^{(0)}$ of the LOS delay parameters $\tau_0^{(0)}$ and $\Delta\tau^{(0)}$ by solving the overdetermined linear system of equations

$$-2\pi \begin{bmatrix} (\Delta f_{n_2^1} - \Delta f_{n_1^1}) & (n_2^1 f_{n_2^1} - n_1^1 f_{n_1^1}) \\ \vdots & \vdots \\ (\Delta f_{n_2^I} - \Delta f_{n_1^I}) & (n_2^I f_{n_2^I} - n_1^I f_{n_1^I}) \end{bmatrix} \begin{bmatrix} \hat{\tau}_0^{(0)} \\ \Delta\hat{\tau}^{(0)} \end{bmatrix} = \begin{bmatrix} \angle\hat{h}_{n_2^1}[0] - \angle\hat{h}_{n_1^1}[0] \\ \vdots \\ \angle\hat{h}_{n_2^I}[0] - \angle\hat{h}_{n_1^I}[0] \end{bmatrix} \tag{15}$$

using the Moore-Penrose pseudoinverse.[3] The n-th channel's

[2]Thus, unlike OFDM-SDF [13], [14], OFDM-based FDA-SDF does not exploit OFDM subcarriers for distributed transmission or frequency diversity, hence preserving all design flexibility benefits of FDA-SDF, as in [15], [16].

[3]Note that the proposed approach allows simultaneous estimation of $\tau_0^{(0)}$ and $\Delta\tau^{(0)}$ from the CIR, as opposed to OFDM-SDF [14] that requires separate estimation of the former, limited in resolution by the sampling frequency.

LOS component estimation is then defined from the estimated delays as

$$\hat{H}_n^{los} = e^{-j2\pi f_n(\hat{\tau}_0^{(0)} + n\Delta\hat{\tau}^{(0)})}. \tag{16}$$

For unambiguous LOS delay estimation from (15), the expected LOS phase difference (14) must not exceed the interval $[-\pi, \pi]$. By noting that unambiguous LOS reconstruction is relevant only within the low BER geocast delivery zone around target coordinates $(d^{steer}, \theta^{steer})$ and that $\tau_0^{(0)} = \frac{d}{c}$, $\Delta\tau^{(0)} = -\frac{b}{c}\sin\theta$, for $b \ll d$ and c the speed of light, (14) yields that only antenna pairs (n_1, n_2) that satisfy the condition

$$\left| -\left(\Delta f_{n_2} - \Delta f_{n_1}\right) d^{steer} + \left(n_2 f_{n_2} - n_1 f_{n_1}\right) b \sin\theta^{steer} \right| < \frac{c}{2} \tag{17}$$

should be considered in (15). Additionally, (13) shows that multipath disturbance on the CIR first tap phase differences in (15) – and hence on the LOS component estimation (16) – decreases as the bandwidth B or the delay differences $\Delta\tau_n^{(l)}$ between multipaths and LOS increase, and vice versa. Therefore, a trade-off between communication bandwidth, channel characteristics (LOS clearance), and SDF robustness applies when designing an FDA-SDF system for multipath scenarios.

III. Measurement Setup

The presented FDA-SDF schemes are validated experimentally using an SDR setup. Precisely, three NI USRP-2954R units are used – two equipping a pair of antennas each to form a linear transmitter array of $N = 4$ antennas and one equipping a single-antenna receiver. They are synchronized in time and frequency through an NI CDA-2990 clock distribution device. All baseband processing, including frequency offset up and down-conversion, is performed in MATLAB on a standard workstation. It is connected to the SDRs via an NI PXIe-1082 chassis for further RF processing at an IQ sampling rate of $F_s = 100$ MHz. The transmitter array consists of a single row from a 4×4 planar patch antenna array with uniform half-wavelength spacing for the employed base carrier frequency $f_c = 5.6$ GHz. At the receiver, a vertical dipole antenna is used. For FDA operation, an alternating linear frequency offset scheme is adopted as defined in [15], with base frequency offset $\Delta f = 10$ MHz. The transmitted datastream consists of 10^5 bits mapped onto a 16-QAM constellation. Transmitter and receiver gains are configured to approximate a 25 dB SNR.

A. Anechoic Chamber

For validation of the free space FDA-SDF system model from Section II-A, the setup is placed within an anechoic chamber, as shown in Fig. 2. The receiver antenna is mounted on a linear axis attached to a turntable at 4.9 m from the transmitter array. In this way, the receiver is moved through a range-azimuth grid, with respective step sizes of 0.025 m and 0.1°, centered around the steering range and angle of, respectively, $d^{steer} = 4.9$ m and $\theta^{steer} = 3°$, measuring the BER at each position. A Hann window is used as the matched filter waveform $g(t)$, yielding a more favorable frequency response than the rectangular window in [15], [16] without violating orthogonality in (5b). The symbol rate is set to $F_d = 5$ MHz.

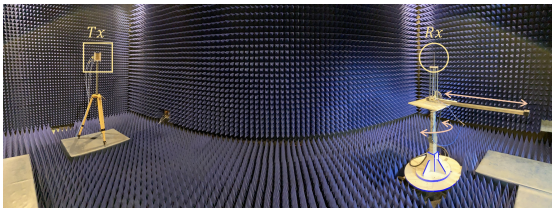

Fig. 2. FDA-SDF anechoic chamber measurement setup.

Fig. 3. FDA-SDF outdoor measurement setup.

B. Outdoors

The multipath FDA-SDF system model from Section II-B is validated in an outdoor suburban-like environment, as shown in Fig. 3. The receiver is mounted on a linear axis oriented either perpendicular (as in Fig. 3) or parallel to the array, for independent 1-dimensional BER measurements in the radial and azimuthal domain, respectively. In both cases, the receiver is moved with a linear step size of 0.05 m along the axis, which is centered around the steering range and angle of, respectively, $d^{steer} = 5.1$ m and $\theta^{steer} = 0°$. Considering the trade-off between SDF robustness and OFDM communication bandwidth from Section II-B3, the latter is set to $B = 10$ MHz. As in [14], LDPC channel coding and semi-inverted Gray code symbol mapping are applied to combat bit errors due to potential imperfect multipath equalization in (12).

IV. Results & Performance Evaluation

A. Anechoic Chamber

Fig. 4 shows the measured 2-dimensional BER distribution for the free space FDA-SDF scheme in the anechoic chamber scenario, compared to its free space simulation. It displays the successful generation of a bounded and isolated low BER geocast delivery zone around the target location. In doing so, it provides the first-ever reported experimental validation of both SDF and – to the best of the authors' knowledge – FDA range-angle-based focusing. It therefore demonstrates the practical achievability of time-invariant FDA when combined with orthogonal baseband signal processing as in FDA-SDF, despite earlier RF FDA models being invalidated by [9]. Due to minor calibration imperfections and residual multipath reflections, e.g. on the receiver stand, a slight spatial shift and more ragged contour of the geocast delivery zone is observed in the experimental results. Nevertheless, the experimental radial and azimuthal geocast delivery zone size, respectively 0.9 m$\pm$ 0.05 m and 4.0° $\pm$ 0.2°, closely approximate their simulated counterparts, respectively 0.875 m $\pm$ 0.05 m and 3.4° $\pm$ 0.2°.

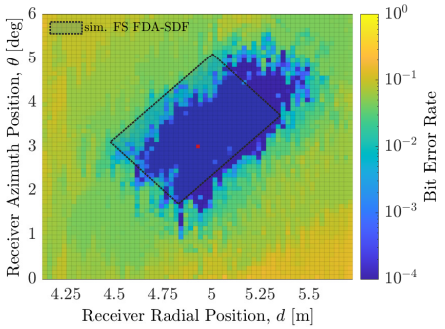

Fig. 4. Spatial BER distribution of FDA-SDF in anechoic chamber scenario with $N = 4$ antennas. Red dot marks target position ($d^{steer} = 4.9$ m, $\theta^{steer} = 3°$).

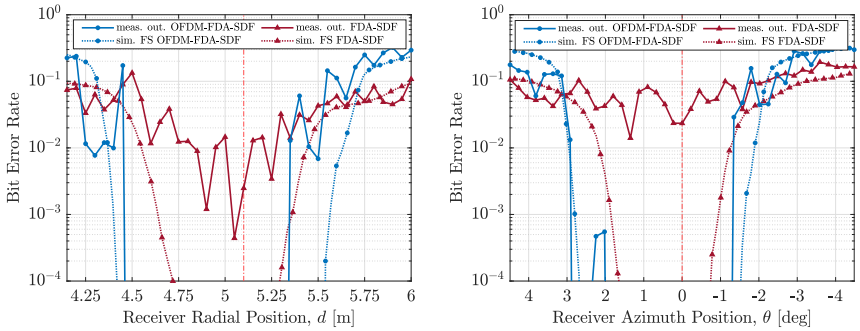

Fig. 5. Radial (left) and azimuthal (right) BER distribution of FDA-SDF in outdoor scenario with $N = 4$ antennas. Red dash-dotted line marks target range ($d^{steer} = 5.1$ m) and angle ($\theta^{steer} = 0°$), respectively.

B. Outdoors

Fig. 5 shows the measured 1-dimensional radial and azimuthal BER distributions for both the free space and multipath FDA-SDF schemes in the outdoor scenario, compared to their respective free space simulations. As anticipated in Section II-B, the free space FDA-SDF scheme cannot operate in multipath environments as it is unable to generate any region of low BER. On the other hand, the proposed multipath FDA-SDF scheme succeeds in re-establishing a low BER geocast delivery zone around the target coordinates, demonstrating its increased robustness and thus the potential for practical FDA-SDF operation. Similarly to [14], the multipath FDA-SDF scheme exhibits a slightly widened geocast delivery zone due to undesired bit error correction beyond its edge by the employed LDPC channel coding.

V. Conclusion and Perspectives

In this paper, the first-ever experimental validation of both spatial data focusing (SDF) and time-invariant frequency diverse array (FDA) range-angle-based focusing is presented. In the context of physical layer geocasting, i.e. spatially confined broadcasting, a hybrid FDA-based SDF (FDA-SDF) approach is considered. After review of the base FDA-SDF free space system model, a novel OFDM-based FDA-SDF approach is proposed to overcome the former's shortcomings in multipath scenarios. Using software defined radios, the schemes' practical performance is assessed in an anechoic chamber and outdoor measurement setup. The former confirms FDA-SDF's supreme spatial focusing precision: a $0.9\,\mathrm{m} \times 4.0°$ range-azimuth geocast delivery zone is generated by a 4-antenna array. The latter demonstrates OFDM-based FDA-SDF's increased robustness and hence prospects for practical operation. Most importantly, SDF's inherent orthogonal baseband signal processing is proven to enable time-invariant FDA operation, thus identifying FDA-SDF geocasting as a viable alternative to previously invalidated RF FDA approaches.

References

[1] C. Maihofer, "A survey of geocast routing protocols," *IEEE Communications Surveys & Tutorials*, vol. 6, no. 2, pp. 32–42, Second Quarter 2004.

[2] N. Sidiropoulos, T. Davidson, and Z.-Q. Luo, "Transmit beamforming for physical-layer multicasting," *IEEE Transactions on Signal Processing*, vol. 54, no. 6, pp. 2239–2251, Jun. 2006.

[3] Y. Zhang, H.-M. Wang, Z. Ding, and M. H. Lee, "Non-orthogonal multiple access assisted multi-region geocast," *IEEE Access*, vol. 6, pp. 2340–2355, Dec. 2018.

[4] P. Antonik, M. Wicks, H. Griffiths, and C. Baker, "Frequency diverse array radars," in *2006 IEEE Conference on Radar*, Verona, NY, USA, Apr. 2006, pp. 215–217.

[5] W. Khan, I. M. Qureshi, and S. Saeed, "Frequency diverse array radar with logarithmically increasing frequency offset," *IEEE Antennas and Wireless Propagation Letters*, vol. 14, pp. 499–502, 2015.

[6] Y. Liu, H. Ruan, L. Wang, and A. Nehorai, "The random frequency diverse array: A new antenna structure for uncoupled direction-range indication in active sensing," *IEEE Journal of Selected Topics in Signal Processing*, vol. 11, no. 2, pp. 295–308, Mar. 2017.

[7] J. Hu, S. Yan, F. Shu, J. Wang, J. Li, and Y. Zhang, "Artificial-noise-aided secure transmission with directional modulation based on random frequency diverse arrays," *IEEE Access*, vol. 5, pp. 1658–1667, 2017.

[8] B. Qiu, J. Xie, L. Wang, and Y. Wang, "Artificial-noise-aided secure transmission for proximal legitimate user and eavesdropper based on frequency diverse arrays," *IEEE Access*, vol. 6, pp. 52 531–52 543, 2018.

[9] Y. Ding, A. Narbudowicz, and G. Goussetis, "Physical limitation of range-domain secrecy using frequency diverse arrays," *IEEE Access*, vol. 8, pp. 63 302–63 309, Mar. 2020.

[10] S. Ji, W.-Q. Wang, H. Chen, and S. Zhang, "On physical-layer security of FDA communications over rayleigh fading channels," *IEEE Transactions on Cognitive Communications and Networking*, vol. 5, no. 3, pp. 476–490, Mar. 2019.

[11] S. Ke, M. He, X. Bu, and W. Cai, "A leakage-based directional modulation scheme for frequency diverse array in robot swarm networks," *IEEE Access*, vol. 8, pp. 107 823–107 837, Jun. 2020.

[12] G. Molineaux, S. Golstein, M. Odhiambo, F. Horlin, P. De Doncker, and J. Sarrazin, "Spatial data focusing using time and IQ resources for wireless geocasting," in *2019 IEEE Global Communications Conference (GLOBECOM)*, Waikoloa, HI, USA, Dec. 2019.

[13] G. Molineaux, M. Odhiambo, F. Horlin, P. De Doncker, and J. Sarrazin, "OFDM-based spatial data focusing for high resolution 2-dimensional wireless geocasting," in *2020 IEEE 31st Annual International Symposium on Personal, Indoor and Mobile Radio Communications*, London, United Kingdom (Great Britain), Aug. 2020, pp. 1–6.

[14] G. Molineaux, F. Horlin, P. De Doncker, and J. Sarrazin, "OFDM-based spatial data focusing for wireless physical layer geocasting in multipath channels," *IEEE Transactions on Wireless Communications*, vol. 21, no. 7, pp. 5064–5074, Jul. 2022.

[15] ——, "Frequency diverse array spatial data focusing for high precision range-angle-based geocasting," in *2022 IEEE Global Communications Conference (GLOBECOM)*, Rio de Janeiro, Brazil, Dec. 2022.

[16] ——, "A spatial data focusing and generalized time-invariant frequency diverse array approach for high precision range-angle-based geocasting," *arXiv:2302.12595*, Feb. 2023.